Research Square

Preprints are preliminary reports that have not undergone peer review.
They should not be considered conclusive, used to inform clinical practice,
or referenced by the media as validated information.

On-Chip Ultrafast Electrons in Asymmetric Nanogaps: a Scalable Platform for Time-Resolved Spectroscopy of Individual Nanosystems

Artem Bakulin

a.bakulin@imperial.ac.uk

Imperial College London https://orcid.org/0000-0002-3998-2000

Haoqing Ning

Imperial College London

Marios Maimaris

Imperial College London

Longren Li

Imperial College London

Jiewen Wei

Imperial College London

Emilie Gérouville

University of Southampton https://orcid.org/0000-0003-2569-5198

Evangelos Moutoulas

University of Southampton

Vladimir Shilovskikh

Leibniz Institute for Solid State and Materials Research Dresden

Oliver Burman

Imperial College London

Zhu Meng

Imperial College London

Clement Ferchaud

Imperial College London

Dmitry Maslennikov

Imperial College London

Navendu Mondal

Imperial College London https://orcid.org/0000-0001-5002-9678

Tong Wang

Imperial College London

Colin Chow

Imperial College London
Aleksandar Ivanov
Imperial College London https://orcid.org/0000-0003-1419-1381
Joshua Edel
Imperial College London https://orcid.org/0000-0001-5870-8659
Saif Haque
Imperial College London https://orcid.org/0000-0001-5483-3321
Misha (Mikhail) Ivanov
Max-Born Institute https://orcid.org/0000-0002-8817-2469
Fabian Paulus7
Leibniz Institute for Solid State and Materials Research Dresden
Yana Vaynzof
Leibniz Institute for Solid State and Materials Research Dresden
Jonathan Marangos
Imperial College London https://orcid.org/0000-0001-7169-6955
Dimitra Georgiadou
University of Southampton https://orcid.org/0000-0002-2620-3346

Article

Keywords:

Posted Date: June 2nd, 2026

DOI: https://doi.org/10.21203/rs.3.rs-7312423/v1

License: This work is licensed under a Creative Commons Attribution 4.0 International License.
Read Full License

Additional Declarations: There is **NO** Competing Interest.

Abstract

Femtosecond-duration and nanometre-size pulses of electrons are emerging as unique probes for ultrafast dynamics at the nanoscale. Such pulses are achievable only in highly sophisticated ultrafast electron microscopes or equally complex setups involving phase-stable few-cycle pulsed lasers and nanotip probes. Here, we show that nanoscale femtosecond pulses of tunnelling electrons can be achieved routinely using any (deep-UV to mid-IR) femtosecond laser in combination with photosensitive asymmetric nanogap (PAN) diodes fabricated via easy-to-scale adhesion lithography technique. The work function difference in PAN electrodes allows generation of electron pulses via strong-field emission without reliance on optical phase stability or external voltage, greatly simplifying and improving sensitivity of the measurements. We apply PANs to measure sub-ps dynamics in individual metal-halide perovskite quantum dots and zinc oxide nanoparticles immobilised inside 10-nm nanogaps and to characterise laser pulses across the entire optical region (266-6500 nm). Short electron pulses in PANs open the way towards scalable on-chip femtosecond electron measurements and novel design approaches for integrated ultrafast nanodevices.

Introduction

Rapid advances in nanotechnology call for new disruptive approaches to characterise molecular systems and materials with extreme temporal and spatial resolution. Nanoscale probing can be achieved using electrons, similarly to the widely used transmission electron microscopy and scanning tunnelling microscopy (STM). To achieve temporal resolution, the probe electrons should be produced and detected in short bunches, rather than as continuous particle beams.

Over the last two decades, the ability of ultrafast lasers to manipulate electrons with high precision in both time and space has exhibited remarkable potential for probing molecular dynamics.[1,2] Operating within picosecond to attosecond time scales, electron-probe techniques could track the processes on the level down to individual atoms and molecules, providing more direct access to previously underexplored issues in material fundamental properties and device physics.[3-6] These issues encompass microscopic ultrafast spin dynamics,[7] nanoscale current transport,[8] quantum light source properties,[9] observation of excitonic states in low-dimensional materials,[10] and the operational mechanisms of individual biological structures.[11] Efforts in the field of time-resolved electron nanoscopy have primarily focused on developing powerful but bulky and highly sophisticated techniques that integrate commercial electron microscopy instruments with ultrafast lasers.[12,13] Several alternative approaches have been proposed, where electrons are generated and/or detected at the nanoscale[14-16] using metal-insulator-metal structures, such as the nanotip emitters, STM machinery,[17-19] and on-chip platforms.[20] These approaches have been successfully applied to measure nanoscale carrier dynamics in semiconductor materials and molecules with sub-nanometre resolution.[21,22]

Nanoscale electron emitters, such as laser-illuminated nanotips[23-26], in combination with macroscale electron detection are currently a mature field. The emission probabilities can be predicted based on a framework similar to one derived for strong-field laser ionisation and high-harmonic generation and can be described using the Keldysh ionisation theory.[27] Based on the Fowler-Nordheim (F-N) field-emission mechanism, nanotip electron emission shows no apparent correlation between the electron emission efficiency and photon energy, easing the constraints on the viable optical sources.[28] The photoelectron spectrum and pulse duration can be further controlled using ω-2ω field shaping,[29] which also partly relaxes the requirement for CEP stabilisation.[30,31] While all this makes nanotips an attractive source of electron pulses, the collection of probe electrons and the application of this approach to characterisation and spectroscopy is still a complex task. Further advancements in electron collection and mapping are necessary to implement these emitters in high throughput nanoscopic measurements.

The use of tunnelling nanostructures has emerged as a robust and scalable approach to achieve high-throughput characterisation of ultrafast dynamics in nanoscale systems. It has the potential to transform and expand many fields currently relying on tunnelling probes – from ultrafast electronics[32] to single-molecule biosensors.[33,34] Nevertheless, a number of limitations needs to be overcome for efficient ultrafast on-chip sensing. The key limitation is based on the fact that short current pulses are generated in nanostructures using the strong (Keldysh parameter $\gamma \leq 1$) alternating electric field of ultrafast optical pulses.[35] However, when the optical field exhibits temporal symmetry (e.g., for multicycle ultrashort pulses) and a nanostructure with symmetrical tunnelling barrier is irradiated, an alternating flow of electrons produces negligible net direct current (DC). To address this challenge, various 'photocurrent rectification' strategies have been employed. The most successful was utilising temporally asymmetric optical fields, such as near-IR[17] or terahertz[18] laser pulses with few optical cycles and controlled carrier-envelope phase (CEP).[8,17,20] Such methods may provide non-zero net tunnelling currents leading to demonstration of sub-femtosecond ultrafast STM with nm spatial resolution.[36] However, few-cycle CEP stabilised lasers are currently expensive and require specialist expertise to operate, limiting application as a general and scalable analytical tool.

An alternative approach to generate pulses of tunnelling current, not requiring sophisticated CEP-stabilised apparatus, relied on applying bias voltages to introduce the asymmetry in nanostructures' current-voltage characteristics to achieve the partial rectification of alternating current generated by the optical field.[19,37] Unfortunately, this latter approach is prone to low-frequency thermal modulation of dark tunnelling current in the nanostructure[38-40] due to plasmonic heating, leading to artefacts, reduced detectivity, and impacting the temporal resolution of the experiments.[41]

A straightforward and robust approach to generate short nanoscale electron pulses would be via nanodevices bearing asymmetric work function electrodes. Combining such structures with ultrashort pulses would enable the generation of sub-cycle electrons from intense optical fields across a broad spectral range, with arbitrary pulse shape and duration.[28,42-44] Given the significant reduction in the

requirements for the optical field, including no need for few-cycle pulses with CEP stabilisation, asymmetric work function devices can be seamlessly integrated into most conventional experimental setups, simplifying ultrafast nanoscale electron probes for molecular-scale spectroscopy. However, the scalable and reliable manufacturing of such nanodevices presents significant challenges; when based on electron beam lithography or scanning probe microscopy techniques, fabrication becomes expensive and low-throughput.[45]

In this study, we employ asymmetric on-chip nanostructures to generate and utilise ultrafast tunnelling current pulses. These nanostructure devices, known as photosensitive asymmetric nanogaps (PANs), are fabricated using adhesion lithography, a simple, high-yield, and cost-efficient coplanar nanogap fabrication technique.[46] Electron pulses in PANs were generated upon irradiation of the nanogap with different ultrafast lasers, without either CEP stabilisation or the need for external voltage bias. PANs performance, reminiscent of a double Schottky diode with a sub-10-nm empty-gap tunnelling barrier, demonstrated rectification of optically induced current under short-pulse illumination. By tuning the wavelength from 266 to 6500 nm and the pulse duration from <10 fs to >100 fs, we show that ultrafast pulses of electrons are produced by the Fowler-Nordheim field emission, rather than thermal expansion, thermoelectric effects, or multi-photon assisted tunnelling. We demonstrate the practical use of PANs for optical detection, tracking the ultrafast electronic dynamics in individual nanosystems located in the nanogap, suggesting broad future applications of PANs technology.

Photosensitive Asymmetric Nanogaps (PANs)

To achieve CEP-free and bias-free photoinduced tunnelling currents, we engineered[47] PANs, metal-nanogap-metal diodes with an asymmetric structure. A planar quasi-2D gold-insulator-aluminium structure is fabricated through adhesion lithography on a glass substrate (Fig. 1, a-d, Supplementary Note 1 for fabrication details). This technique enables the easy and high-throughput fabrication of arrays of asymmetric metal electrodes with large aspect ratios without requiring costly and time-consuming processes and equipment, such as e-beam lithography.[46] Asymmetric electrodes fabricated with adhesion lithography have been used in GHz radiofrequency diodes,[48] fast photodetectors,[49] organic light-emitting diodes,[50] and memory devices[51], including ferroelectric tunnel junctions.[52] However, the strong-field effects at these nanochannels have not been studied so far.

The PAN chips are composed of a glass substrate covered by a thin (40 nm) layer of aluminium. The Al film does not cover the substrate completely; 1-mm square ‘islands’ of gold (40 nm thickness) are periodically patterned on the substrate, each Au island separated from aluminium by a nanogap. (Fig. 1a) The length of each nanogap is equal to the island’s perimeter (~4 mm) and the width of the gap is ~10 nm based on SEM, TEM (Fig. 1,c,d) and previous work.[47] During the experiment, only a part of the gap (typically 50 mm in length) was illuminated by ultrafast laser pulses.

The significant nominal offset (~1.2 eV) in work functions of the metal counterparts (Au vs Al) (Fig. 1a, inset) leads to strong current rectification properties of PANs due to the asymmetric and nonlinear

response to the external electric field. For instance, this effect can be seen, in the *J-V* characteristics measured without laser irradiation from -3 V to +3 V (Fig. 1e and Supplementary Fig. 1). The minimal current flow in the reverse bias regime as well as the exponential increase in current at ~1.2 V in the forward direction is reminiscent of diode characteristics. Although the electron emission rate depends upon the optical field direction the inherent asymmetry ensures there is a net photocurrent.

Under continuous-wave laser illumination, we did not observe any photocurrent (Supplementary Fig. 2), indicating the device is not susceptible to heating-induced current modulation, which is one of the key effects limiting externally-biased optically-assisted STM approaches.[53,54] Upon ultrafast laser irradiation (with intensities ~10^{10} W cm^{-2} and above), the *J-V* characteristics of the PAN change (Fig. 1e), showing a distinct photocurrent response in on-off tests (Fig. 1f). This suggests optical activation of tunnelling electrons emission via the strong electric field which is potentially further enhanced by plasmonic effects (Fig. 1g). As measurements are done at zero applied bias and CW illumination does not produce photocurrent, the measurement of ultrafast light with PANs can be considered background free. This allows PANs to routinely detect photocurrents down to 10 fA (1-5 electrons per pulse), which is highly challenging in biased electronic devices (Supplementary Fig. 4).

Mechanism of photocurrent generation in PANs

To explore the limits of PANs' applicability and to investigate the mechanism behind the electron pulses, we have studied the efficiency of photocurrent generation depending on the photon energy, pulse energy, and pulse duration. We test the nanogap using various ultrafast laser systems (Supplementary Fig. 5, Supplementary Table S1), encompassing wavelengths ranging from 266 nm (deep-UV) to 6.5 μm (mid-IR), with pulse durations varying from ~8 fs to over 100 fs.

Fig. 2a presents the dependencies of photocurrent on the radiant exposure for the different laser systems used in the absence of the external bias voltage. Across a very broad UV-to-IR spectral range, under ~0.2-20 mJ/cm^2 illumination, photocurrents in the range of ~0.3-30 pA are achieved across the nanogap. At higher illuminations, photocurrents up to 0.5 nA were achieved (Supplementary Fig. 3), though we avoided using this regime not to compromise the device stability. The presented curves are roughly linear in log-log plot and can be fitted by the power law function with the power indexes ranging between 1.7 and 3.4. The 2-fold variation in the power index is much smaller than the 15-fold variation in the incident photon energy, indicating that the underlying mechanism is unlikely to be based on a multiphoton process. Different slopes were observed for lasers of similar wavelengths, indicating that both the light pulse intensity and duration affect the systems' behaviour. Our measurements indicate that the peak light intensities (and, correspondingly, the peak electric field in the nanogap) rather than photons' energies play the dominant role in the photocurrent generation. When the power index (the exponent of power dependence) is plotted as a function of the calculated peak electric field achieved by the optical pulse, the results from all laser systems follow a single trend (Fig. 2b), which can be well reproduced using a field emission model discussed below.

To identify the specific mechanism governing the generation of ultrafast photocurrents, we considered the signal dependence on the key experiment parameters, namely the light wavelength, external voltage, and peak field strength. The potential factors that may contribute to the photocurrent are: (i) slow modulation of the barrier due to thermal expansion and related phenomena; (ii) multiphoton-assisted tunnelling below the barrier energy; (iii) multiphoton-assisted electron emission with photon energy surpassing the barrier, or (iv) Fowler-Nordheim emission via modulation of the ionisation barrier by a strong optical field.

The non-linear response of photocurrent upon illumination and its weak dependence on the illumination wavelength indicates that sample heating and heat-induced nanogap modulation have negligible contributions to the observed signals (see Supplementary Note 8 and Supplementary Fig. 6 in SI). Photon-assisted tunnelling can be considered an alternative mechanism, however, our calculations of photon-assisted tunnelling currents for pulsed optical fields based on Bessel solution through Tien-Gorden theory (see SI, Supplementary Note 9) contradict the experimental data. The theory predicts a much higher order power law (power index of ~8) for photocurrent dependence on illumination, compared to the power indexes of 1.6-3.5 observed in the experiment (Fig. 2a).

Finally, we consider electron emission mechanisms via strong-field ionisation barrier modulation and multiphoton ionisation (Supplementary Notes 7 and 8). By taking the work function of electrodes as the equivalent to ionisation energy of a gas, we find the Keldysh parameter is between 0.001 and 2.54 (Supplementary Fig. 12), suggesting that most of our experimental data lie within the strong-field rather than the multiphoton region.[55] Consequently, we conclude that the variations in the barrier induced by the optical field and the subsequent emission of electrons dominate the photocurrent generation.

Fig. 2c shows how F-N mechanism leads to the generation of a rectified current pulse in the oscillating field of an optical pulse and illustrates its predictive power. After tunneling from the surface of the aluminium/gold interface, electrons enter a strong near-field gradient. Depending on the precise timing of emission relative to the laser field oscillation, the electron experiences either acceleration or deceleration. These sub-cycle or quiver trajectories lead to an attosecond electron pulse train (see also Supplementary Fig. 16).

Fig. 2d shows the photocurrent generated in PAN by 800-nm 35-fs optical pulses as a function of irradiation fluence and external bias. Notably, the photocurrent is present even at zero bias, with its amplitude and direction being further controlled by the applied voltage. The photocurrent dependence on irradiating flux still follows a power law, but increased bias gradually diminishes the value of the power index (see SI, Supplementary Figs. 13 and 14), until the current becomes negligible and then changes sign at the open-circuit voltage. All the observed trends can be reproduced (Supplementary Figs. 10 and 11) with a F-N field-emission model.

Broadband ultrafast pulse autocorrelation measurements with PANs

The transfer of field-emission electron pulses across a ~10-nm gap is expected to occur at sub-cycle timescales (Fig. 2c and Supplementary Fig. 15) making the electron pulses very short and thus an attractive ultrafast probe for both irradiating optical fields and the intra-gap environment. We verify the fast response time of PANs using optical autocorrelation, as the process is too fast to be measured using electronic detection.

Fig. 2e-g presents baseline-corrected two-pulse intensity autocorrelation under non-collinear geometry. All the autocorrelation traces demonstrate symmetric shapes and no long-lived component in the signals, indicating the fast response and absence of an electronic population built-up or heating effects. For 800-nm pulses, we compared photocurrent autocorrelation to the BBO second harmonic generation (SHG) autocorrelation measurement and, after the correction for nonlinear order, observed a good agreement between the data (Fig. 2f). This was achieved without any need to satisfy phase-matching conditions in PAN, highlighting the possible applicability of tunnelling-based detection for characterisation of short and broadband pulses in IR and deep UV range (See also Supplementary Figs. 18-20), where the use of non-linear crystals can be problematic (Fig. 2e,g).[56] To demonstrate the robustness of the approach, we systematically varied the pre-chirp in the amplifier and successfully monitored the alteration in the shape of the optical pulse (Supplementary Fig. 17). The above pulse characterisation involves modest laser powers, a low level of non-linearity, and no need for CEP stabilisation or sub-10fs compression, which makes PANs more versatile and accessible than existing state-of-the-art pulse sampling techniques.[57]

Mapping individual nanosystems in PANs

The possibility of generating ultrafast nanoscale photocurrent pulses in PANs carries a clear potential for nanoscale spectroscopy applications. The generated electrons can be used to probe the electronic and structural dynamics of molecular-scale systems entrapped in the nanogap. The fact that electrons can be generated by light of practically any wavelength makes this approach highly flexible and versatile. The optical-pump electron-probe spectroscopy, has been previously demonstrated for STM-based systems.[18] We extend this approach to monitor charge dynamics in nanosystems within the PAN's 10-nm channel.

Fig. 3 shows that individual small (~10-nm) $CsPbBr_3$ quantum dots (QDs) can be deposited and detected in the PANs channel. Using an air brush technique in combination with dielectrophoretic (DEP) trapping (see SI, Supplementary Note 19 for experimental details and material characterisation), we deposited highly diluted QDs on the PANs chip (Fig. 3a) and then detected the presence of individual QDs in the nanogap using photoluminescence microscopy (Fig. 3b,d,g) and electron tunnelling pulses (Fig. 3c,f,h,i). Fig. 3d shows composite bright-dark field microscopy images of the nanogap after DEP-assisted deposition of QDs. Bright field scattering signal reveals the location of the borderline (nanogap) between Al and Au electrodes and dark field measurement. The bright spots in the image show emissive nano objects located within and outside the nanogap. Time-dependent emission of the object located in the nanogap demonstrate clear blinking behaviour (Fig. 3g) indicating that it likely originates from a single

perovskite nanocrystal. Also, upon DEP deposition of $CsPbBr_3$ QDs, the dark tunnelling current in the PAN changes due to the changes in the tunnelling barrier, consequently leading to alterations in the *J-V* curves (Fig. 3e). This confirms that a significant number of deposited 10-nm QDs reside within the nanogap.

Fig. 3g-i demonstrate that individual QDs can be spatially resolved within the nanogap by combining optical microscopy illumination (3 mm focal spot, 800-nm, 35-fs pulses) with detection of optically induced tunnelling currents. The top panel of Fig. 3h shows a microscopic map of the tunnelling current in an empty nanogap, prior to QD deposition. The nanogap is clearly identifiable, and the induced photocurrents typically range from 1 to 3 pA. In contrast, after QD deposition (bottom panel), multiple localized hotspots appear within the nanogap. These hotspots exhibit photocurrent amplitudes of 4-8 pA and are randomly distributed along the gap, with clear spatial separation from one another. This strongly suggests that the hotspots correspond to individual QDs embedded in the nanogap. Further evidence for the formation of new tunnelling hotspots is provided in Fig. 3i, which presents a statistical comparison of photocurrent distributions in empty and QD-deposited nanogaps. A distinct sub-population of high-current hotspots emerges upon QD deposition. Fig. 3f zooms in on one such hotspot using a higher-resolution microscopy scan. The signal is sharply localized on a sub-micrometer scale, likely due to the nonlinear nature of the photocurrent response.

Ultrafast electronic dynamics in the nanocrystals can be monitored using a pump–probe experiment with tunnelling current detection (Fig. 4). In this scheme, a weak resonant pump pulse photoexcites the material within the nanogap without directly inducing tunnelling. Subsequently, an intense non-resonant probe pulse generates tunnelling electrons, enabling the detection of changes in the excited-state dynamics of the nanomaterial without directly exciting it electronically. The tunnelling probe is sensitive to the electronic state of the system, as photoexcitation alters the tunnelling barrier and likely influences the trajectories of field-emitted electrons (Fig. 4a).

We first demonstrate the tunnelling barrier modulation effect by studying electronic dynamics in the bulk film of ZnO filling up the gap (Fig. 4b). We used 400 nm pump pulses for above-gap excitation of the material and 6.5 mm as below-gap probe. ZnO is transparent in mid-IR, therefore this probe did not interact with ZnO directly, but generated electron pulses in the PAN. As the concentration of the excited states promptly goes up after photoexcitation and then decays on multiple timescales (from 200 fs to 10s of ps) due to recombination, we observed the change in tunnelling current at timescales that are in agreement with earlier studies.[47,58]

We also demonstrate the mapping of electronic dynamics in individual QDs deposited in the nanogap (Fig. 4c-h). We employed 35-fs 400 nm pulses as excitation and similarly short 800 nm pulses for generating tunnelling-electron probe. Fig. 4c shows time traces measured by microscopy excitation beam focusing on individual QD in the nanogap. Upon excitation, we observed that the photocurrent amplitude rapidly increases by ~0.2 pA and then decays on <10 ps time scales. The rapid signal rise corresponds to excitation of electrons to the QD conduction band. The observed decay times are shorter

than carrier lifetimes reports based on transient absorption measurements in QD films (Supplementary Fig. 27 and Fig. 28).[59] The fastest timescale of ~300 fs aligns with the dynamics of carrier cooling in perovskite nanomaterials[59] and with photoconductivity measurements on perovskite thin films obtained via transient terahertz spectroscopy[60]. The slower decay component observed in PAN/tunneling measurements indicates a significantly accelerated decay in nanocavity-coupled single-QD systems, potentially driven by Purcell enhancement. We, therefore, attribute the observed signal to the formation of hot carriers, followed by their cooling, extraction, and recombination.[61-64]

By scanning the pump and probe beams along the nanogap (Fig. 4d-g), we can identify individual nanosystems and monitor their distinct dynamics (Fig. 4h), generating dynamic maps similar to those produced by far more sophisticated ultrafast STM measurements.[10,65] These results demonstrate fast and scalable time-resolved characterisation of individual nanosystems. High-throughput measurements can be performed by scanning along the gap from one photocurrent hotspot to another and by addressing different nanojunctions on the chip. We observed that PANs approach readily achieves temporal information down to <15-fs (Supplementary Fig. 29) which is much faster than what can be achieved by THz STM or PL-based spectroscopy techniques[66]. PANs can also be applied for the detection and characterisation of non-emissive individual nanosystems such as $AgBiS_2$ QDs (Supplementary Note 20, Supplementary Fig. 26), which are inaccessible to widely used PL microscopy tools.

Conclusion

The presented results show that combining on-chip asymmetric nanogap structures, PANs, with ultrafast illumination provides a versatile method to generate ultrafast pulses of tunnelling electrons via the broadband Fowler-Nordheim photoelectron emission. PANs are fabricated using an inexpensive, simple, and high-throughput technique, called adhesion lithography, and operate without the need for CEP stabilisation or an external electric bias, making them applicable in any ultrafast laser lab. We have also demonstrated the practical use of PANs for broadband characterisation of optical pulses and ultrafast spectroscopy of individual nanoobjects (e.g. perovskite QDs, $AgBiS_2$ QDs, and ZnO nanocrystals) as model systems. The herein developed approach opens new research avenues in photonics, including nonlinear-crystal-free optical pulse characterisation and nanoscale imaging. We anticipate that PANs will emerge as a cost-effective, durable, and adaptable foundation for integrated ultrafast broadband optoelectronics and for ultrafast spectroscopy on individual nanosystems.

Declarations

Acknowledgements

We thank Maxim Pchenitchnikov and Ernest Pastor for valuable discussions. John Tisch is acknowledged for providing a photonic fibre 10-fs laser source. We thank Lea Haase for providing the

$AgBiS_2$ nanocrystals. AAB acknowledges support from the Royal Society via the University Research Fellowship and Leverhulme Trust via the Philip Leverhulme Prize award. This project received funding from the European Research Council (ERC) under the European Union's Horizon 2020 research and innovation program (Grant Agreement 639750/VIBCONTROL) and from UKRI/EPSRC (ActionSpec, grant ref: EP/X030822/1). FP thanks the German Federal Ministry of Research, Technology and Space (BMFTR) for funding (FK 03XP0422A). The project was also supported by the EPSRC New Horizons Grant (TRON, grant ref: EP/V049070/1). Dmitry R. Maslennikov acknowledges funding by the Imperial College London President's PhD Scholarships. CF and JPM acknowledge funding support from UKRI/EPRSC EP/V026690/1, EP/T006943/1, and EP/R019509/1. DGG and EM acknowledge support from the UKRI Future Leaders Fellowship Grant (MR/V024442/1).

References

1. Zewail, A. H. 4D ultrafast electron diffraction, crystallography, and microscopy. *Annual Review of Physical Chemistry* **57**, 65–103 (2006). https://doi.org/10.1146/annurev.physchem.57.032905.104748
2. Schiffrin, A. *et al.* Optical-field-induced current in dielectrics. *Nature* **493**, 70–74 (2013). https://doi.org/10.1038/nature11567
3. Cocker, T. L., Peller, D., Yu, P., Repp, J. & Huber, R. Tracking the ultrafast motion of a single molecule by femtosecond orbital imaging. *Nature* **539**, 263–267 (2016). https://doi.org/10.1038/nature19816
4. Fu, X., Chen, B., Tang, J., Hassan, M. T. & Zewail, A. H. Imaging rotational dynamics of nanoparticles in liquid by 4D electron microscopy. *Science* **355**, 494–498 (2017). https://doi.org/doi:10.1126/science.aah3582
5. Mohammed, O. F., Yang, D.-S., Pal, S. K. & Zewail, A. H. 4D Scanning Ultrafast Electron Microscopy: Visualization of Materials Surface Dynamics. *Journal of the American Chemical Society* **133**, 7708–7711 (2011). https://doi.org/10.1021/ja2031322
6. Davis, T. J. *et al.* Ultrafast vector imaging of plasmonic skyrmion dynamics with deep subwavelength resolution. *Science* **368**, eaba6415 (2020). https://doi.org/doi:10.1126/science.aba6415
7. Kirilyuk, A., Kimel, A. V. & Rasing, T. Ultrafast optical manipulation of magnetic order. *Rev Mod Phys* **82**, 2731–2784 (2010). https://doi.org/10.1103/RevModPhys.82.2731
8. Ludwig, M. *et al.* Sub-femtosecond electron transport in a nanoscale gap. *Nature Physics* (2019). https://doi.org/10.1038/s41567-019-0745-8
9. Gutzler, R., Garg, M., Ast, C. R., Kuhnke, K. & Kern, K. Light–matter interaction at atomic scales. *Nature Reviews Physics* **3**, 441–453 (2021). https://doi.org/10.1038/s42254-021-00306-5
10. Plankl, M. *et al.* Subcycle contact-free nanoscopy of ultrafast interlayer transport in atomically thin heterostructures. *Nature Photonics* **15**, 594–600 (2021). https://doi.org/10.1038/s41566-021-00813-y

11. Flannigan, D. J., Barwick, B. & Zewail, A. H. Biological imaging with 4D ultrafast electron microscopy. *Proceedings of the National Academy of Sciences* **107**, 9933–9937 (2010). https://doi.org/doi:10.1073/pnas.1005653107
12. Baum, P., Yang, D.-S. & Zewail, A. H. 4D Visualization of Transitional Structures in Phase Transformations by Electron Diffraction. *Science* **318**, 788–792 (2007). https://doi.org/doi:10.1126/science.1147724
13. Miller, R. J. D. Femtosecond Crystallography with Ultrabright Electrons and X-rays: Capturing Chemistry in Action. *Science* **343**, 1108–1116 (2014). https://doi.org/doi:10.1126/science.1248488
14. Park, D. J. *et al.* Strong Field Acceleration and Steering of Ultrafast Electron Pulses from a Sharp Metallic Nanotip. *Physical Review Letters* **109**, 244803 (2012). https://doi.org/10.1103/PhysRevLett.109.244803
15. Li, S. & Jones, R. R. High-energy electron emission from metallic nano-tips driven by intense single-cycle terahertz pulses. *Nature Communications* **7**, 13405 (2016). https://doi.org/10.1038/ncomms13405
16. Dombi, P. *et al.* Strong-field nano-optics. *Rev Mod Phys* **92**, 025003 (2020). https://doi.org/10.1103/RevModPhys.92.025003
17. Garg, M. & Kern, K. Attosecond coherent manipulation of electrons in tunneling microscopy. *Science* **367**, 411–415 (2020). https://doi.org/doi:10.1126/science.aaz1098
18. Cocker, T. L. *et al.* An ultrafast terahertz scanning tunnelling microscope. *Nature Photonics* **7**, 620–625 (2013). https://doi.org/10.1038/Nphoton.2013.151
19. Terada, Y., Yoshida, S., Takeuchi, O. & Shigekawa, H. Real-space imaging of transient carrier dynamics by nanoscale pump–probe microscopy. *Nature Photonics* **4**, 869–874 (2010). https://doi.org/10.1038/nphoton.2010.235
20. Bionta, M. R. *et al.* On-chip sampling of optical fields with attosecond resolution. *Nature Photonics* **15**, 456–460 (2021). https://doi.org/10.1038/s41566-021-00792-0
21. Böckmann, H. *et al.* Valley-controlled photoswitching of metal–insulator nanotextures. *Nature Physics* (2025). https://doi.org/10.1038/s41567-025-02899-5
22. Zizlsperger, M. *et al.* In situ nanoscopy of single-grain nanomorphology and ultrafast carrier dynamics in metal halide perovskites. *Nature Photonics* **18**, 975–981 (2024). https://doi.org/10.1038/s41566-024-01476-1
23. Arashida, Y. *et al.* Subcycle Mid-Infrared Electric-Field-Driven Scanning Tunneling Microscopy with a Time Resolution Higher Than 30 fs. *ACS Photonics* **9**, 3156–3164 (2022). https://doi.org/10.1021/acsphotonics.2c00995
24. Vogelsang, J. *et al.* Ultrafast Electron Emission from a Sharp Metal Nanotaper Driven by Adiabatic Nanofocusing of Surface Plasmons. *Nano Lett* **15**, 4685–4691 (2015). https://doi.org/10.1021/acs.nanolett.5b01513
25. Hommelhoff, P., Sortais, Y., Aghajani-Talesh, A. & Kasevich, M. A. Field Emission Tip as a Nanometer Source of Free Electron Femtosecond Pulses. *Physical Review Letters* **96**, 077401 (2006).

https://doi.org/10.1103/PhysRevLett.96.077401

26. Barwick, B. *et al.* Laser-induced ultrafast electron emission from a field emission tip. *New Journal of Physics* **9**, 142 (2007). https://doi.org/10.1088/1367-2630/9/5/142
27. Kim, H. Y. *et al.* Attosecond field emission. *Nature* **613**, 662–666 (2023). https://doi.org/10.1038/s41586-022-05577-1
28. Herink, G., Solli, D. R., Gulde, M. & Ropers, C. Field-driven photoemission from nanostructures quenches the quiver motion. *Nature* **483**, 190–193 (2012). https://doi.org/10.1038/nature10878
29. Haché, A. *et al.* Observation of Coherently Controlled Photocurrent in Unbiased, Bulk GaAs. *Physical Review Letters* **78**, 306–309 (1997). https://doi.org/10.1103/PhysRevLett.78.306
30. Dienstbier, P. *et al.* Tracing attosecond electron emission from a nanometric metal tip. *Nature* **616**, 702–706 (2023). https://doi.org/10.1038/s41586-023-05839-6
31. Meier, S., Heimerl, J. & Hommelhoff, P. Few-electron correlations after ultrafast photoemission from nanometric needle tips. *Nature Physics* **19**, 1402–1409 (2023). https://doi.org/10.1038/s41567-023-02059-7
32. Krüger, M., Schenk, M. & Hommelhoff, P. Attosecond control of electrons emitted from a nanoscale metal tip. *Nature* **475**, 78–81 (2011). https://doi.org/10.1038/nature10196
33. Mauranyapin, N. P., Madsen, L. S., Taylor, M. A., Waleed, M. & Bowen, W. P. Evanescent single-molecule biosensing with quantum-limited precision. *Nat Photonics* **11**, 477–481 (2017). https://doi.org/10.1038/nphoton.2017.99
34. Clarke, J. *et al.* Continuous base identification for single-molecule nanopore DNA sequencing. *Nature Nanotechnology* **4**, 265–270 (2009). https://doi.org/10.1038/nnano.2009.12
35. Rybka, T. *et al.* Sub-cycle optical phase control of nanotunnelling in the single-electron regime. *Nature Photonics* **10**, 667–670 (2016). https://doi.org/10.1038/nphoton.2016.174
36. Garg, M. *et al.* Real-space subfemtosecond imaging of quantum electronic coherences in molecules. *Nature Photonics* **16**, 196–202 (2022). https://doi.org/10.1038/s41566-021-00929-1
37. Yoshida, S. *et al.* Probing ultrafast spin dynamics with optical pump–probe scanning tunnelling microscopy. *Nature Nanotechnology* **9**, 588–593 (2014). https://doi.org/10.1038/nnano.2014.125
38. Grafstrom, S., Schuller, P., Kowalski, J. & Newmann, R. Thermal expansion of scanning tunneling microscopy tips under laser illumination. *J Appl Phys* **83**, 3453–3460 (1998). https://doi.org/Doi 10.1063/1.366556
39. Gerstner, V., Knoll, A., Pfeiffer, W., Thon, A. & Gerber, G. Femtosecond laser assisted scanning tunneling microscopy. *J Appl Phys* **88**, 4851–4859 (2000). https://doi.org/Doi 10.1063/1.1290706
40. Xie, N. *et al.* Tip expansion in a laser assisted scanning tunneling microscope. *Appl Phys Lett* **101** (2012). https://doi.org/Artn 213104 10.1063/1.4767877
41. Dolocan, A., Acharya, D. P., Zahl, P., Sutter, P. & Camillone, N. Two-Color Ultrafast Photoexcited Scanning Tunneling Microscopy. *J Phys Chem C* **115**, 10033–10043 (2011). https://doi.org/10.1021/jp111875f

42. Putnam, W. P., Hobbs, R. G., Keathley, P. D., Berggren, K. K. & Kärtner, F. X. Optical-field-controlled photoemission from plasmonic nanoparticles. *Nature Physics* **13**, 335–339 (2017). https://doi.org/10.1038/nphys3978
43. Frolov, M. V. *et al.* Analytic Description of the High-Energy Plateau in Harmonic Generation by Atoms: Can the Harmonic Power Increase with Increasing Laser Wavelengths? *Physical Review Letters* **102**, 243901 (2009). https://doi.org/10.1103/PhysRevLett.102.243901
44. Echternkamp, K. E. *et al.* Strong-field photoemission in nanotip near-fields: from quiver to sub-cycle electron dynamics. *Applied Physics B* **122**, 80 (2016). https://doi.org/10.1007/s00340-016-6351-x
45. Li, T., Hu, W. & Zhu, D. Nanogap Electrodes. *Advanced Materials* **22**, 286–300 (2010). https://doi.org/10.1002/adma.200900864
46. Beesley, D. J. *et al.* Sub-15-nm patterning of asymmetric metal electrodes and devices by adhesion lithography. *Nature Communications* **5**, 3933 (2014). https://doi.org/10.1038/ncomms4933
47. Georgiadou, D. G. *et al.* 100 GHz zinc oxide Schottky diodes processed from solution on a wafer scale. *Nature Electronics* **3**, 718–725 (2020). https://doi.org/10.1038/s41928-020-00484-7
48. Semple, J. *et al.* Large-area plastic nanogap electronics enabled by adhesion lithography. *npj Flexible Electronics* **2**, 18 (20Not). https://doi.org/10.1038/s41528-018-0031-3
49. Georgiadou, D. G. *et al.* High Responsivity and Response Speed Single-Layer Mixed-Cation Lead Mixed-Halide Perovskite Photodetectors Based on Nanogap Electrodes Manufactured on Large-Area Rigid and Flexible Substrates. *Advanced Functional Materials* **0**, 1901371 (2019). https://doi.org/10.1002/adfm.201901371
50. Wyatt-Moon, G., Georgiadou, D. G., Zoladek-Lemanczyk, A., Castro, F. A. & Anthopoulos, T. D. Flexible nanogap polymer light-emitting diodes fabricated via adhesion lithography (a-Lith). *Journal of Physics: Materials* **1**, 01LT01 (2018). https://doi.org/https://doi.org/10.1088/2515-7639/aadd57
51. Raeis-Hosseini, N., Georgiadou, D. G. & Papavassiliou, C. High On/Off Ratio Carbon Quantum Dot–Chitosan Biomemristors with Coplanar Nanogap Electrodes. *ACS Applied Electronic Materials* **5**, 138–145 (2023). https://doi.org/10.1021/acsaelm.2c00979
52. Kumar, M. *et al.* Colossal Tunneling Electroresistance in Co-Planar Polymer Ferroelectric Tunnel Junctions. *Advanced Electronic Materials* **6**, 1901091 (2020). https://doi.org/https://doi.org/10.1002/aelm.201901091
53. Hoffmann, D., Seifritz, J., Weyers, B. & Moller, R. Thermovoltage in scanning tunneling microscopy. *J Electron Spectrosc* **109**, 117–125 (2000). https://doi.org/Doi 10.1016/S0368-2048(00)00111-0
54. Grafström, S. Photoassisted scanning tunneling microscopy. *J Appl Phys* **91**, 1717–1753 (2002). https://doi.org/10.1063/1.1432113
55. Lewenstein, M., Balcou, P., Ivanov, M. Y., L'Huillier, A. & Corkum, P. B. Theory of high-harmonic generation by low-frequency laser fields. *Physical Review A* **49**, 2117–2132 (1994). https://doi.org/10.1103/PhysRevA.49.2117
56. Lee, J. P. *et al.* Few-femtosecond soft X-ray transient absorption spectroscopy with tuneable DUV-Vis pump pulses. *Optica* **11**, 1320–1323 (2024). https://doi.org/10.1364/OPTICA.530964

57. Sederberg, S. *et al.* Attosecond optoelectronic field measurement in solids. *Nature Communications* **11**, 430 (2020). https://doi.org/10.1038/s41467-019-14268-x
58. Bauer, C., Boschloo, G., Mukhtar, E. & Hagfeldt, A. Ultrafast relaxation dynamics of charge carriers relaxation in ZnO nanocrystalline thin films. *Chemical Physics Letters* **387**, 176–181 (2004). https://doi.org/https://doi.org/10.1016/j.cplett.2004.01.106
59. Carwithen, B. P. *et al.* Confinement and Exciton Binding Energy Effects on Hot Carrier Cooling in Lead Halide Perovskite Nanomaterials. *ACS Nano* **17**, 6638–6648 (2023). https://doi.org/10.1021/acsnano.2c12373
60. Kumar, A. *et al.* Excitons in 2D perovskites for ultrafast terahertz photonic devices. *Science Advances* **6**, eaax8821 (2020). https://doi.org/doi:10.1126/sciadv.aax8821
61. Ma, Q. *et al.* Tuning ultrafast electron thermalization pathways in a van der Waals heterostructure. *Nature Physics* **12**, 455–459 (2016). https://doi.org/10.1038/nphys3620
62. Chen, J., Messing, M. E., Zheng, K. & Pullerits, T. Cation-Dependent Hot Carrier Cooling in Halide Perovskite Nanocrystals. *Journal of the American Chemical Society* **141**, 3532–3540 (2019). https://doi.org/10.1021/jacs.8b11867
63. Chung, H. *et al.* Composition-Dependent Hot Carrier Relaxation Dynamics in Cesium Lead Halide (CsPbX3, X=Br and I) Perovskite Nanocrystals. *Angewandte Chemie International Edition* **56**, 4160–4164 (2017). https://doi.org/https://doi.org/10.1002/anie.201611916
64. Mondal, N. & Samanta, A. Complete ultrafast charge carrier dynamics in photo-excited all-inorganic perovskite nanocrystals (CsPbX3). *Nanoscale* **9**, 1878–1885 (2017). https://doi.org/10.1039/C6NR09422H
65. Luo, Y. *et al.* Visualizing hot carrier dynamics by nonlinear optical spectroscopy at the atomic length scale. *Nature Communications* **16**, 4999 (2025). https://doi.org/10.1038/s41467-025-60384-2
66. Neef, A. *et al.* Orbital-resolved observation of singlet fission. *Nature* **616**, 275–279 (2023). https://doi.org/10.1038/s41586-023-05814-1

Figures

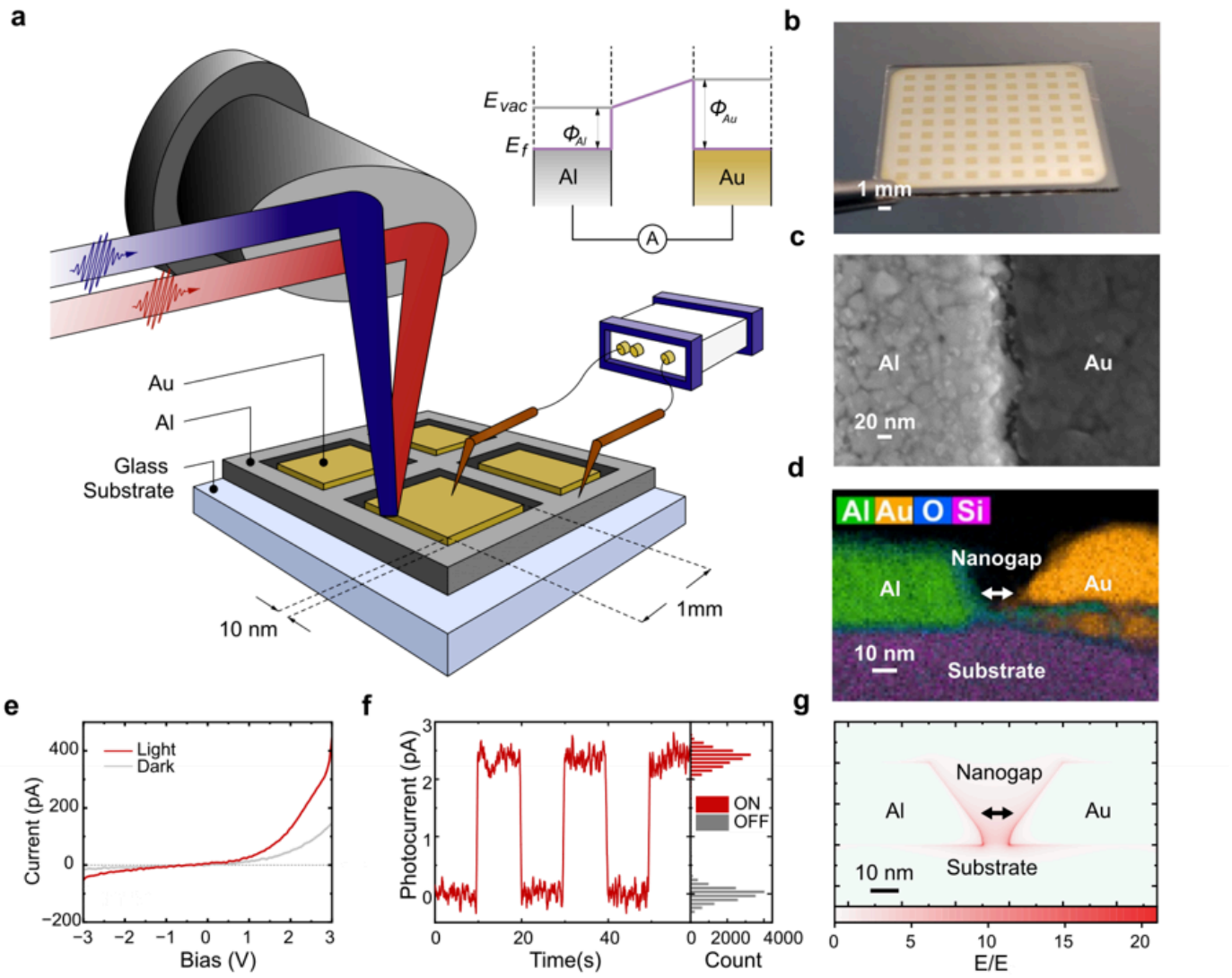


Figure 1

Strong-field tunnelling in a PAN device: a) *Schematic of an Au–nanogap–Al PAN device under ultrafast optical excitation. Inset - Energy band diagram of the nanogap diode composed of Al and Au electrodes illustrating the inherent asymmetry in their work functions.* ***b)*** *Photograph showing a 9x9 array of nanogap devices fabricated on a single chip.* ***c)*** *SEM image of the Au–Al nanogap.* ***d)*** *Cross-sectional TEM image of the nanogap region, with elemental mapping confirming Au–Al interfaces and nanogap width.* ***e)*** *J-V characteristics of PAN diode with/without illumination.* ***f)****Representative photocurrent trace under 1030 nm, 190 fs, 10 kHz pulsed laser irradiation at 0 V bias, showing binary on/off behaviour and corresponding statistical distribution with 30 ms time averaging.* ***g)*** *FDTD simulation of plasmonic field enhancement under 10 fs 1450 nm excitation.*

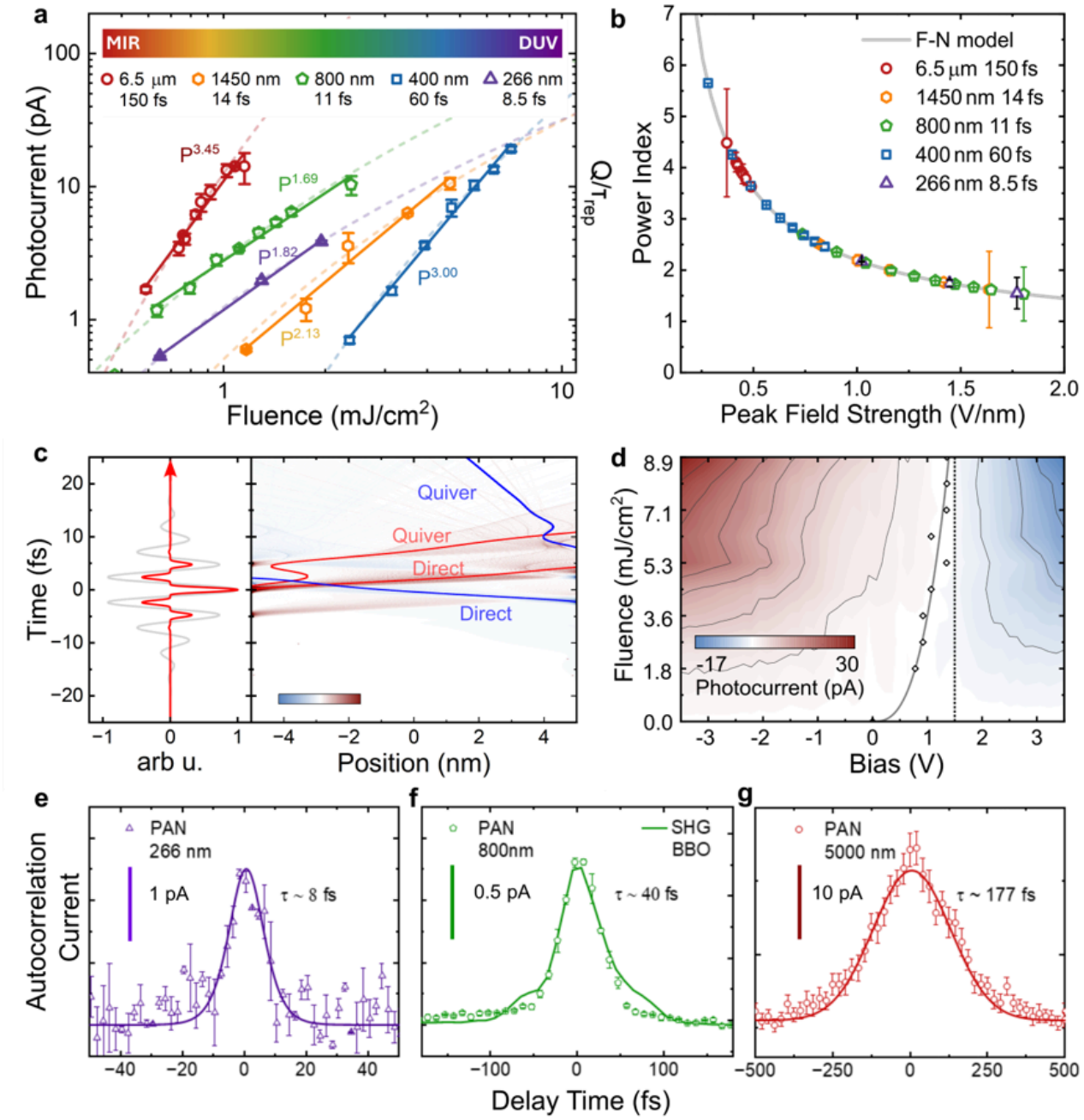


Figure 2

Optically induced currents in PAN devices: a) Ultrafast laser-induced photocurrents at zero external bias. Different colours/scatters correspond to experiments on various laser systems with different wavelengths of irradiating light (from UV to IR) and pulse durations. The solid lines are power-law fits to the data with the power index indicated. The dashed lines are the fits using the F-N field-emission model. b) Nonlinear power index and peak field strength calculated based on a) and field emission model, based on the wavelength, focal spot size, pulse energy, and pulse duration in different experiments. The solid line represents a global fit using the field-emission model for all experimental data collected across the optical spectrum. c) Semi-classical (simple-man) simulation of strong-field tunnelling: left, electric field waveform; right, electron trajectories across a 10 nm gap. Colour encodes the initial yield of electrons, with direct and quiver

trajectories indicated. d) The 2D map of the amplitude of photocurrent under 800-nm 35-fs illumination as a function of external bias, V_b, and illuminating fluence, F. The diamond line marks the minimum photocurrent position. e-g) Autocorrelation traces of laser pulses used in the experiments: e) ~8 fs, 266 nm deep UV pulses measured in vacuum (~10^{-6} mbar); f) ~40 fs, 800 nm pulses with comparison to second-harmonic autocorrelation in a BBO crystal (solid line); g) ~170 fs, 5 μm MIR pulses. All measurements were performed under zero electrical bias.

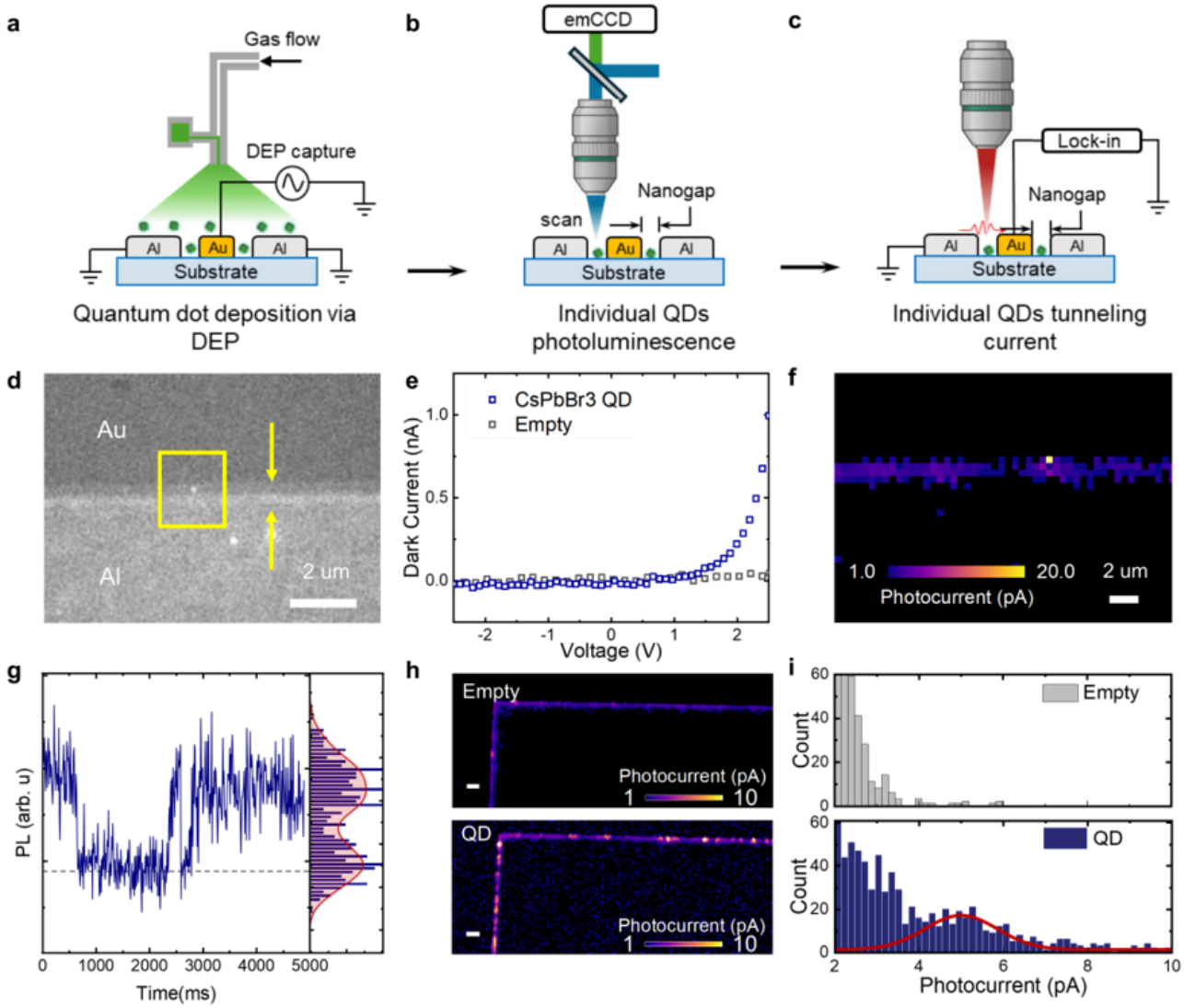


Figure 3

Mapping individual QDs in PANs. a) *DEP assisted airbrush spraying is used to trap low-concentration QDs (~nM) onto PANs. J–V scans are performed to monitor possible conductance changes induced by the deposition.* ***b)*** *Confocal hybrid/dark-field photoluminescence (PL) microscopy image on PAN with deposited QDs.* ***c)*** *Ultrafast tunneling photocurrent detection used to localize individual QDs within the PANs.* ***d)*** *Confocal image showing isolated QDs on a PAN chip.* ***e)*** *J–V characteristics comparing PANs with few deposited QDs versus empty PANs.* ***f)*** *Sub radius (0.7 NA, 400 nm step size) tunneling photocurrent imaging map locating individual QD in PANs.* ***g)****Representative two-state PL blinking behavior of a single QD.* ***h)***

Ultrafast tunnelling current mapping and comparison between empty and QD-deposited PANs. Scale bar is 20 μm. ***i)*** *Statistical distribution of tunneling counts before and after QD deposition.*

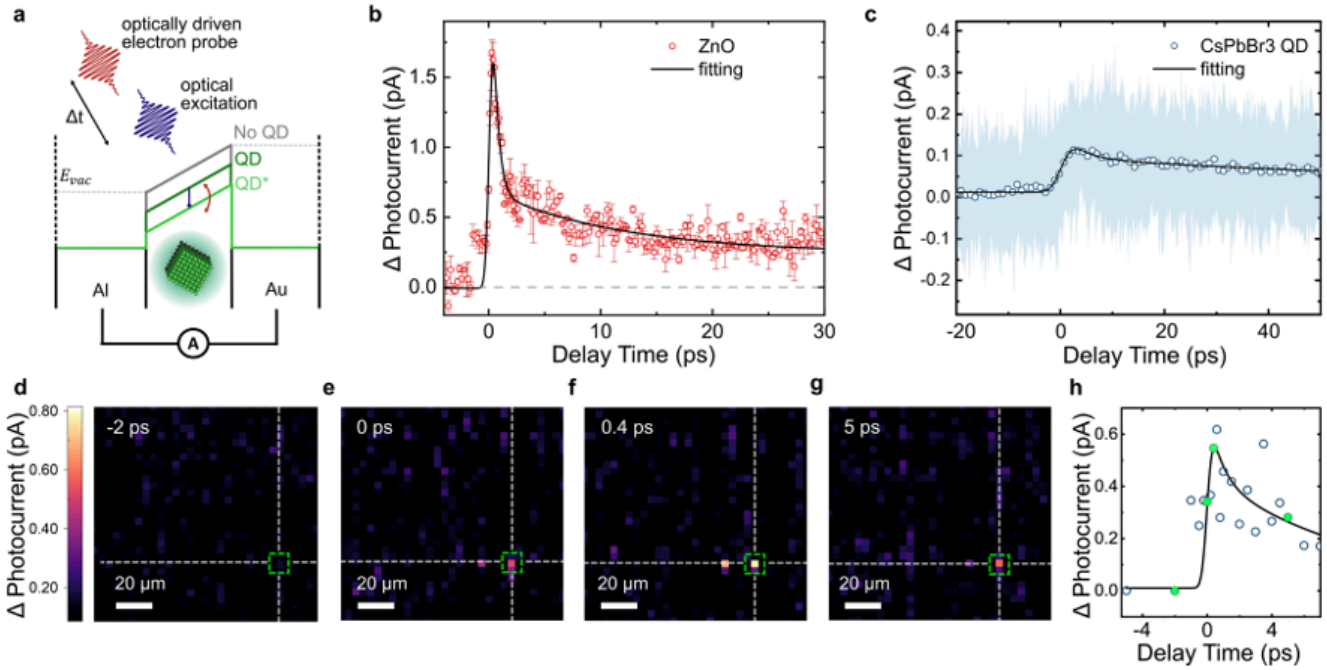


Figure 4

Mapping dynamics of ZnO and individual QDs in PANs. a) *Schematic of the optical pump tunnelling-photocurrent probe with adjustable delay Δt. The excited state of the nanosystem modifies the tunneling barrier and modulates the tunneling current.* ***b)*** *Ultrafast tunneling photocurrent change in a 10 nm, ZnO-coated diode upon optical excitation of ZnO.* ***c)*** *Ultrafast tunnelling photocurrent change in a single $CsPbBr_3$ QD upon QD optical excitation; blue circles present the average over 40 scans.* ***d-g)*** *Time-resolved pump-probe ΔI maps at selected delay times (−2 ps, 0 ps, 0.4 ps, 5 ps), highlighting the localisation of pump-probe signal.* ***h)*** *Pump-probe ΔI dynamics in the QD region of the map. Green dots correspond to specific maps presented in d-g). In all panels black lines are bi-exponential fits convoluted with Gaussian response function. All time-resolved data are corrected for the baselines at negative times.*

Supplementary Files

This is a list of supplementary files associated with this preprint. Click to download.

- supplementaryPANs.docx